Radiative Transfer in Spectrally Dissimilar Absorbing-Emitting-Scattering Adjacent Mediums

K. H. Im* and R. K. Ahluwalia*
Argonne National Laboratory, Argonne, Illinois

The structure of a radiation field in a cylindrical medium having two regions of different but uniform absorption and scattering coefficients is analyzed. Fundamental aspects of the problem are elucidated by considering the case of a gray medium. It is shown, for example, that for unequal absorption coefficients in the two regions, both emission and absorption rates are discontinuous at the interface of the two regions, but the heat flux and incident radiation are continuous. As an application of the analysis, the influence of spatial distribution of particles on heat transfer in a coal-burning swirl combustor is investigated. In the example application, spectral calculations are performed spanning over the broad frequency range of the thermal radiation spectrum.

Nomenclature

a = parameter $\equiv [3(1-\omega)]^{1/2}\beta$
F = function defined in Eq. (17)
g_0 = incident radiation at the interface
G = incident radiation
H = function defined in Eq. (18)
i = $\sqrt{-1}$
I = intensity
I_b = blackbody intensity
I_w = I_b at wall temperature
K = Green's function
m = complex refractive index
n = size distribution function
N_0 = total number density
N = total number
P_l^l = associated Legendre polynomial
Q = efficiency factor
Q_r = heat flux in radial direction
q_0 = heat flux at the interface
r = radial coordinate
r_0 = radius of region 1
r_p = particle radius
$\langle r_p \rangle$ = average radius
R = radius of the combustor
T = temperature
u = flow velocity
Y_ℓ = ℓth-order modified Bessel function of the first kind
Z_ℓ = ℓth-order modified Bessel function of the second kind
α_1 = function defined in Eq. (32)
α_2 = function defined in Eq. (33)
β = extinction coefficient
γ = function defined in Eq. (10)
δ = boundary-layer thickness
ϵ_w = wall emissivity
ϵ_ν = Knudsen number for radiation transport
θ = polar angle
Θ_+ = step function
κ = absorption/scattering coefficient
λ = wavelength
μ = $\cos\theta$
ρ_g = gas density
ρ_p = particle density
ϕ = azimuthal angle of the point under consideration
ϕ' = azimuthal angle (measured from r direction) of the radiation beam
ω = scattering albedo

Subscripts

1 = region 1
2 = region 2
a = absorption
c = core
s = scattering
w = wall
ν = spectral quantity

Introduction

IN many engineering applications, a situation of neighboring regions possessing vastly dissimilar spectral properties is encountered. An example of such a situation is the coal-burning swirl combustor for a magnetohydrodynamic (MHD) power plant. An intention behind imparting swirl to the flow in an MHD combustor is to cause preferential segregation of the coal particles in the low-temperature wall region and, hence, to minimize the vaporization of nonvolatile ash material in the coal. The segregation occurs in regard to both the number density and the average size of the coal particle-size distribution function. The reason for segregation with respect to the number density is the centrifugal force acting on the particles because of the swirl motion. With respect to particle size, smaller particles have short relaxation time and therefore tend to follow the fluid turbulence. The net result is that in spite of the centrifugal force, smaller particles are unable to preferentially collect in the wall region, but remain uniformly suspended. This is true so long as $(R/\ddot{r}_p)^{1/2} > \tau_t > \tau_p$, where R is the radius of combustor, $\ddot{r}_p$ is the centrifugal acceleration of the particle by the mean flow, τ_t is the time scale of turbulence, and τ_p is the particle relaxation time. Thus we have the following situation in high-swirl combustors: the majority of large-size particles segregate in the wall region, while the small-size particles are more or less uniformly distributed over the entire flowfield. From the standpoint of thermal radiation, the small- and large-size particles have quite different absorption and scattering characteristics. Small particles absorb more radiation than they scatter, whereas the opposite is true for the large-size particles. A question then arises as to how the stratification of a large number of scattering (and absorbing) coal particles in the wall region influences the heat transfer characteristics of the swirl combustor. The formulation made in the present work is primarily dedicated to developing the fundamentals needed to answer such a question, but is otherwise very general in scope.

Presented as Paper 81-1091 at the AIAA 16th Thermophysics Conference, Palo Alto, Calif., June 23-25, 1981; submitted Dec. 8, 1981; revision received April 29, 1982.

*Mechanical Engineer, Engineering Division.

The importance of the problem of radiation transport in stratified media is not limited to the swirl combustors only. Stratification also occurs in conventional nonswirl combustors with central injection of coal particles. In this case, segregation occurs in the core region as opposed to the wall region in the swirl combustor. Similarly, the stratification effects are not restricted to the coal combustors only. Stratification effects of a different sort occur in oil combustors in which diffusion flames are present. Here, soot particles that are produced in the flame zone play a dominant role in radiation transport. Over a distance of the order of flame length, the soot particles are expected to be concentrated in the flame region. Beyond this distance, dispersion of soot particles will take place due to the mixing action of fluid turbulence.

One of the difficulties in dealing with radiation problems, in which the particle effects are included, is that the particles absorb and emit radiation of all frequencies. This necessitates solving the radiation transport equation on detailed spectral basis. Since in most problems of practical interest, convection and radiation are generally of equal importance, the necessity of retaining spectral information forces one (for computational reasons) to seek an approximation method for solving the radiation transport equation. This is especially true when the medium under consideration is nonplanar and the scattering effects are to be included. This is precisely the situation being dealt with in the present work. A convenient method of simplifying the solution is the P_1 approximation,[1] which is used in the present work also. In this study, an absorbing, emitting, and scattering medium of cylindrical geometry is considered. The medium is idealized to consist of two regions, each region having spatially uniform spectral properties. The two regions, however, have different spectral properties. Suitable spectral properties are assigned to the two regions so that the question posed earlier can be addressed.

It should be stressed that the P_1 method of solving the radiation transport equation is an approximate one. The accuracy of the P_1 approximation has been assessed by Bayazitoglu and Higenyi[2] for the situation of heat transfer between the walls of concentric cylinders when the medium is in radiative equilibrium. It was found that the P_1 approximation is less exact in the optically thin limit than the thick limit. However, the P_1 solution has correct behavior for all optical path lengths. Therefore, even though results from the present study may be somewhat inaccurate in the optically thin limit, they will always be qualitatively correct.

Formulation of the Problem

Neglecting the axial transfer of heat and assuming isotropic scattering, the spectral intensity I_ν in cylindrical coordinates is governed by the following radiation transport equation:

$$(1-\mu^2)^{1/2}\left(\cos\phi'\frac{\partial I_\nu}{\partial r}+\sin\phi'\frac{1}{r}\frac{\partial I_\nu}{\partial \phi}\right)+\beta_\nu I_\nu$$

$$=(1-\omega_\nu)\beta_\nu I_{b\nu}+\frac{\omega_\nu\beta_\nu}{4\pi}\int_0^{2\pi}\int_{-1}^{1} I_\nu \,d\mu d\phi \qquad (1)$$

A general method of solving Eq. (1) is to expand I_ν in an infinite series, in terms of the spherical harmonic functions. For the purpose of simplification, we invoke the P_1 approximation; accordingly, the infinite series is truncated after the first-order terms so that the following expression for I_ν may be obtained:

$$I_\nu(r,\mu,\phi)=\frac{1}{4\pi}\left[G_\nu(r)+3\cos\phi' P_1^1(\mu)Q_{r\nu}(r)\right] \qquad (2)$$

Where G_ν is the incident radiation

$$G_\nu=\int_{-1}^{1}\int_0^{2\pi} I_\nu \,d\phi' \,d\mu \qquad (3)$$

$Q_{r\nu}$ is the net radiant heat flux in the radial direction

$$Q_{r\nu}=\int_{-1}^{1}\int_0^{2\pi}\cos\phi'(1-\mu^2)^{1/2} I_\nu \,d\phi' \,d\mu \qquad (4)$$

and P_1^1 is the first order associated Legendre polynomial. Furthermore, the heat flux $Q_{r\nu}$ is related to the gradient of the incident radiation as

$$Q_{r\nu}=-\frac{1}{3\beta_\nu}\frac{\partial G_\nu}{\partial r} \qquad (5)$$

Finally, G_ν obeys the following differential equation:

$$\frac{1}{r}\frac{\partial}{\partial r}\left(\frac{r}{\beta_\nu}\frac{\partial G_\nu}{\partial r}\right)-3(1-\omega_\nu)\beta_\nu G_\nu=-12\pi(1-\omega_\nu)\beta_\nu I_{b\nu} \qquad (6)$$

We consider a segregated medium consisting of two regions possessing distinctly different spectral properties. In particular, let the two regions have uniform spectral properties: $\beta_{\nu 1}$ and $\omega_{\nu 1}$ for region 1, and $\beta_{\nu 2}$ and $\omega_{\nu 2}$ for region 2. At the interface of the two regions ($r=r_0$), β_ν and ω_ν are discontinuous. Mathematically, the variations of β_ν and ω_ν in the complete radiation field can be represented by step functions,

$$\beta_\nu=\beta_{\nu 1}+\Delta\beta_\nu\Theta_+(r-r_0) \qquad (7)$$

$$(1-\omega_\nu)\beta_\nu=(1-\omega_{\nu 1})\beta_{\nu 1}+\Delta[(1-\omega_\nu)\beta_\nu]\Theta_+(r-r_0) \qquad (8)$$

Substituting Eqs. (7) and (8) into Eq. (6), the following equations for the incident radiation in regions 1 and 2 are obtained: region 1,

$$\frac{1}{r}\frac{\partial}{\partial r}\left(r\frac{\partial G_{\nu 1}}{\partial r}\right)-3(1-\omega_{\nu 1})\beta_{\nu 1}^2 G_{\nu 1}=-12\pi(1-\omega_{\nu 1})\beta_{\nu 1}^2 I_{b\nu} \qquad (9)$$

region 2,

$$\frac{1}{r}\frac{\partial}{\partial r}\left(r\frac{\partial G_{\nu 2}}{\partial r}\right)-3(1-\omega_{\nu 2})\beta_{\nu 2}^2 G_{\nu 2}=-12\pi(1-\omega_{\nu 2})\beta_{\nu 2}^2 I_{b\nu} \qquad (10)$$

From the requirements of continuity of G_ν (actually of I_ν) and heat flux, the interface boundary conditions are

$$G_{\nu 1}=G_{\nu 2} \text{ at } r=r_0 \qquad (11)$$

$$\frac{1}{\beta_{\nu 1}}\frac{\partial G_{\nu 1}}{\partial r}=\frac{1}{\beta_{\nu 2}}\frac{\partial G_{\nu 2}}{\partial r} \text{ at } r=r_0 \qquad (12)$$

The interface boundary conditions can be derived purely on mathematical basis also by integrating Eq. (6) across a vanishingly thin region about the interface, and using the mean value theorem. Two additional boundary conditions are required to uniquely define the problem. These are the axial symmetry at the centerline,

$$\frac{\partial G_{\nu 1}}{\partial r}=0 \text{ at } r=0 \qquad (13)$$

and the wall boundary condition[3] (the wall is assumed to be diffusely reflecting).

$$\frac{2}{3}\left(\frac{2}{\epsilon_w}-1\right)\frac{1}{\beta_{\nu 2}}\frac{\partial G_{\nu 2}}{\partial r}+G_{\nu 2}=4\pi I_{w\nu} \text{ at } r=R \tag{14}$$

Solutions of Eqs. (9) and (10) subject to boundary conditions (11-14) are pursued in the next section.

Solution of the Problem

It is convenient to first solve separately two subproblems for regions 1 and 2. For region 1, we assume that the spectral intensity at the interface is known; i.e., we solve Eq. (9) subject to boundary condition given by Eq. (13) and assuming that

$$G_{\nu 1}=g_0 \text{ at } r=r_0 \tag{15}$$

For region 2 we assume that the heat flux at the interface is prescribed; i.e.,

$$-\frac{1}{3\beta_\nu}\frac{\partial G_{\nu 2}}{\partial r}=q_0 \text{ at } r=r_0 \tag{16}$$

Then, Eq. (10) is solved for $G_{\nu 2}$ subject to boundary conditions prescribed by Eqs. (14) and (16). At this point, the actual values of g_0 and q_0 are unknown. These are to be computed by matching the solutions for the two regions in accordance with the interface boundary conditions prescribed by Eqs. (11) and (12).

The actual solution proceeds by defining transformed variables, F_ν for region 1 and H_ν for region 2, such that the boundary conditions become homogeneous:

$$F_\nu=G_{\nu 1}-g_0 \tag{17}$$

$$H_\nu=G_{\nu 2}-4\pi I_{w\nu}-3q_0[\beta_{\nu 2}(R-r)+\gamma] \tag{18}$$

where

$$\gamma=\tfrac{2}{3}(2/\epsilon_w-1) \tag{19}$$

The following are the governing equations and the boundary conditions for F_ν and H_ν:

$$\frac{1}{r}\frac{\partial}{\partial r}\left(r\frac{\partial F_\nu}{\partial r}\right)-a_{\nu 1}^2F_\nu=-4\pi a_{\nu 1}^2\left(I_{b\nu}-\frac{g_0}{4\pi}\right) \tag{20}$$

$$\frac{\partial F_\nu}{\partial r}=0 \text{ at } r=0 \tag{21}$$

$$F_\nu=0 \text{ at } r=r_0 \tag{22}$$

$$\frac{1}{r}\frac{\partial}{\partial r}\left(r\frac{\partial H_\nu}{\partial r}\right)-a_{\nu 2}^2H_\nu=3\beta_{\nu 2}\frac{q_0}{r}$$
$$-4\pi a_{\nu 2}^2\left\{I_{b\nu}-I_{w\nu}-\frac{3q_0}{4\pi}[\beta_{\nu 2}(R-r)+\gamma]\right\} \tag{23}$$

$$\frac{\partial H_\nu}{\partial r}=0 \text{ at } r=r_0 \tag{24}$$

$$\frac{\gamma}{\beta_{\nu 2}}\frac{\partial H_\nu}{\partial r}+H_\nu=0 \text{ at } r=R \tag{25}$$

where

$$a_{\nu 1}^2=3(1-\omega_{\nu 1})\beta_{\nu 1}^2, \qquad a_{\nu 2}^2=3(1-\omega_{\nu 2})\beta_{\nu 2}^2$$

Because of the linearity of Eqs. (20) and (23) and homogeneity of their boundary conditions, the solutions for F_ν and H_ν and, hence, for $G_{\nu 1}$ and $G_{\nu 2}$ can be written immediately in terms of the Green's functions:

$$G_{\nu 1}=g_0+\int_0^{r_0}4\pi a_{\nu 1}^2K_{\nu 1}(r\,|r')(I_{b\nu}-g_0/4\pi)r'\,dr' \tag{26}$$

$$G_{\nu 2}=4\pi I_{w\nu}+3q_0[\beta_{\nu 2}(R-r)+\gamma]+\int_{r_0}^{R}K_{\nu 2}(r\,|r')$$
$$\times(-3\beta_{\nu 2}(q_0/r')+4\pi a_{\nu 2}^2\{I_{b\nu}-I_{w\nu}-(3q_0/4\pi)$$
$$\times[\beta_{\nu 2}(R-r')+\gamma]\})r'\,dr' \tag{27}$$

In Eq. (26), $K_{\nu 1}(r\,|r')$ is the Green's function which satisfies Eq. (20) with its right-hand side replaced by the delta function $-(1/r)\delta(r-r')$, subject to the boundary conditions expressed by Eqs. (21) and (22). The following solution for $K_{\nu 1}$ can be constructed:

$$K_{\nu 1}^{+}(r\,|r')=[Z_0(a_{\nu 1}r)-Y_0(a_{\nu 1}r)Z_0(a_{\nu 1}r_0)$$
$$\div Y_0(a_{\nu 1}r_0)]Y_0(a_{\nu 1}r') \qquad r_0>r>r' \tag{28}$$

$$K_{\nu 1}^{-}(r\,|r')=[Z_0(a_{\nu 1}r')-Y_0(a_{\nu 1}r')Z_0(a_{\nu 1}r_0)$$
$$\div Y_0(a_{\nu 1}r_0)]Y_0(a_{\nu 1}r) \qquad r_0<r'<r \tag{29}$$

In the foregoing equations, Y_ℓ stands for the ℓth-order modified Bessel function of the first kind (the usual notation is I_ℓ), and Z_ℓ stands for the ℓth-order modified Bessel function of the second kind (the usual notation is K_ℓ).

Similarly, $K_{\nu 2}(r\,|r')$ in Eq. (27) is the Green's function which satisfies Eq. (23) with its right-hand side replaced by the delta function $-(1/r)\delta(r-r')$, subject to the boundary conditions expressed by Eqs. (24) and (25). After considerable mathematical manipulations, the following solution for $K_{\nu 2}$ may be constructed:

$$K_{\nu 2}^{+}(r\,|r')=\frac{1}{\alpha_2-\alpha_1}[\alpha_1Y_0(a_{\nu 2}r)+Z_0(a_{\nu 2}r)]$$
$$\times[\alpha_2Y_0(a_{\nu 2}r')+Z_0(a_{\nu 2}r')] \qquad r_0>r'>r \tag{30}$$

$$K_{\nu 2}^{-}(r\,|r')=\frac{1}{\alpha_2-\alpha_1}[\alpha_2Y_0(a_{\nu 2}r)+Z_0(a_{\nu 2}r)]$$
$$\times[\alpha_1Y_0(a_{\nu 2}r')+Z_0(a_{\nu 2}r')] \qquad r_0'>r>r \tag{31}$$

where

$$\alpha_1=[\gamma a_{\nu 2}Z_1(a_{\nu 2}R)-\beta_{\nu 2}Z_0(a_{\nu 2}R)]$$
$$\div[\gamma a_{\nu 2}Y_1(a_{\nu 2}R)+\beta_{\nu 2}Y_0(a_{\nu 2}R)] \tag{32}$$

$$\alpha_2=Z_1(a_{\nu 2}r_0)/Y_1(a_{\nu 2}r_0) \tag{33}$$

The two spectral quantities, the incident radiation g_0 and the net heat flux q_0, remain to be determined from the inteface conditions. For Eq. (26), $G_{\nu 1}$ at $r=r_0$ is naturally equal to g_0. Therefore, to determine g_0, we require that $G_{\nu 2}$ at $r=r_0$ be equal to g_0. This gives

$$g_0-q_0\left\{3[\beta_{\nu 2}(R-r_0)+\gamma]-3\int_{r_0}^{R}[\beta_{\nu 2}/r'\right.$$
$$\left.+a_{\nu 2}^2(\beta_{\nu 2}(R-r')+\gamma)]K_{\nu 2}(r_0\,|r')]r'\,dr'\right\}$$
$$=4\pi I_{w\nu}+4\pi\int_{r_0}^{R}a_{\nu 2}^2(I_{b\nu}-I_{w\nu})K_{\nu 2}(r_0\,|r')r'\,dr' \tag{34}$$

In the same manner, the heat flux at $r=r_0$ computed from the $G_{\nu 2}$ equation is naturally equal to q_0, because this fact was used as a boundary condition in deriving Eq. (27). Therefore, to determine q_0 we require that $-1/(3\beta_{\nu 1})\partial G_{\nu 1}/\partial r$ at $r=r_0$ be equal to q_0. This gives

$$q_0+g_0\left\{\frac{1}{3\beta_{\nu 1}r_0Y_0(a_{\nu 1}r_0)}\int_0^{r_0}a_{\nu 1}^2Y_0(a_{\nu 1}r')r'\,dr'\right\}$$

$$=\frac{4\pi}{3\beta_{\nu 1}r_0Y_0(a_{\nu 1}r_0)}\int_0^{r_0}a_{\nu 1}^2I_{b\nu}Y_0(a_{\nu 1}r')r'\,dr' \qquad (35)$$

where we have made use of the following equation:

$$\left(\frac{\partial K_{\nu 1}}{\partial r}\right)_{r=r_0}=-\frac{Y_0(a_{\nu 1}r')}{r_0Y_0(a_{\nu 1}r_0)} \qquad (36)$$

Equations (34) and (35) are linear with respect to the two unknowns, g_0 and q_0, and, hence, are easily solved for them. For brevity, we omit writing the detailed expressions for g_0 and q_0. But once g_0 and q_0 are explicitly defined, Eq. (26) defines the incident radiation field in region 1 and Eq. (27) defines the field in region 2. This completes the solution to our radiation problem.

The various terms in Eqs. (26), (27), (34), and (35) can be physically interpreted as follows. According to Eq. (26), the incident radiation at any point in region 1 is the sum of 1) the incident radiation at the interface (g_0) minus its attenuation during the path from the interface to the point under consideration; and 2) the radiation emitted in region 1 which also suffers attenuation. In Eq. (27), the incident radiation at any point in region 2 is determined by the combined influence of the following effects: a) the radiation emitted by the wall (I_{wp}) and its attenuation; b) the absorption in region 2 of the radiation due to the heat flux incident at the interface; c) the radiation emitted in region 2 which also suffers attenuation; and d) the wall effect, e.g., the reflection of radiation incident at the wall. Equation (35) describes the relationship between g_0 and q_0 from the standpoint of the emission and absorption processes taking place in region 1. Equation (34) also describes the same relationship but from the standpoint of emission and absorption of radiation in region 2 and the wall effect. The interpretation of various terms in Eqs. (34) and (35) follows closely that given earlier in connection with Eqs. (26) and (27).

Results and Discussion

Two sets of results are presented in this study. In the first set, a gray medium assumption is made in order to clarify the physical aspects of the problem. In the second set, detailed spectral calculations are made to probe the influence on heat transfer of the segregation of particles in the near-wall region. In both sets of results, the emissive power of the medium is assumed to be prescribed. In particular, the following temperature profile is assumed to prevail in the boundary layer:

$$\frac{(T-T_w)}{(T_c-T_w)}=\frac{3/2(R-r)}{\delta}-\frac{1/2(R-r)^3}{\delta^3} \qquad (37)$$

where $T_w=1800$ K, $T_c=2800$ K, and $R=1$ m. The qualitative aspects of the results should be independent of the type of temperature profile that is assumed to exist. Quantitatively the results will depend on the temperature profile.

Gray Medium Calculations

In this section, both regions 1 and 2 are assumed to be gray mediums. It is also assumed that $r_0=0.7$ m, $\delta=1$ m, and $\epsilon_w=0.7$. Figure 1 depicts the spatial variation of local heat flux when the regions 1 and 2 have equal absorption coefficients ($\kappa_1=\kappa_2$) but unequal scattering albedoes ($\omega_1\neq\omega_2$). Since the problem is axisymmetric, the local heat flux is zero at the centerline. It is seen first to increase with the radial distance and then to decrease. In the region where the local heat flux decreases with radial distance, the divergence of radiant heat flux is negative; i.e., this is a strongly absorbing region. The extent of the region in which strong absorption takes place is of course a function of the assumed temperature profile. Figure 1 also shows the influence of ω_2 on heat flux when κ_1, κ_2, and ω_1 are held fixed. Increasing ω_2 is seen to diminish the heat flux at all points in the radiation field and to distend the region in which strong absorption occurs. It is also observed that with respect to increase in ω_2, the decrease in local heat flux is much greater in the strong absorption region (negative divergence of heat flux) than in the strong emission region (positive divergence of heat flux). The effect of ω_2 on the divergence of heat flux, a quantity that determines how fast the gas is being radiatively cooled or heated, is more clearly evident in the next sketch.

For the conditions of Fig. 1 the spatial variations of the absorption ($\kappa G/4\pi$) and emission (κI_b) rates are shown in Fig. 2. The difference between the emission and absorption rates gives the divergence of heat flux. In the region where the emission rate exceeds the absorption rate, the divergence of heat flux is positive and the gas cools down. The opposite is true wherever the emission is exceeded by the absorption rate. Since $\kappa_1=\kappa_2$ and the emissive power is fixed and continuous, the emission rate in Fig. 2 is seen to be independent of ω_2 and to be continuous across the interface ($r_0/R=0.7$). As ω_2 is varied, it is the incident radiation (G) that gets affected. Figure 2 shows that G generally increases with ω_2 except very close to the wall. The intersection of the absorption and emission rate curves demarcate the strong emission region (cooling zone) from the strong absorption region (heating zone). Figure 2 illustrates that the extent of the heating zone is distended with ω_2—a trend that was noted previously. Finally, since $\kappa_1=\kappa_2$ and G have to be continuous at the interface, the absorption rate also turns out to be continuous in the calculations represented in Fig. 2.

Figure 3 depicts the spatial variation of local heat flux when $\kappa_1\gg\kappa_2$ and $\omega_1\neq\omega_2$. Even though the spectral coefficients have a step-function variation, the heat flux is seen to be continuous, as is expected from the physics of the problem. The

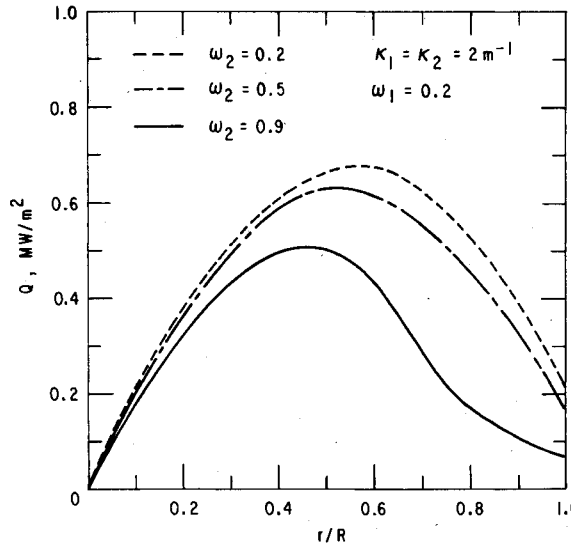

Fig. 1 Effect of ω_2 on heat flux ($\kappa_1=\kappa_2$, $\omega_1\neq\omega_2$).

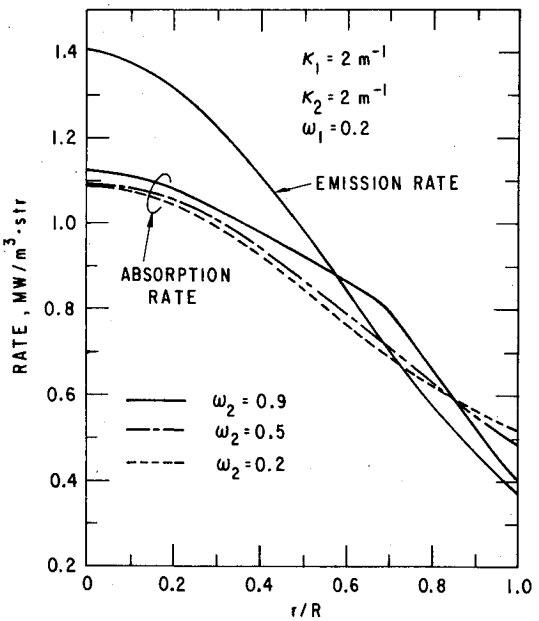

Fig. 2 Spatial variations of absorption and emission rates ($\kappa_1 = \kappa_2$, $\omega_1 \neq \omega_2$).

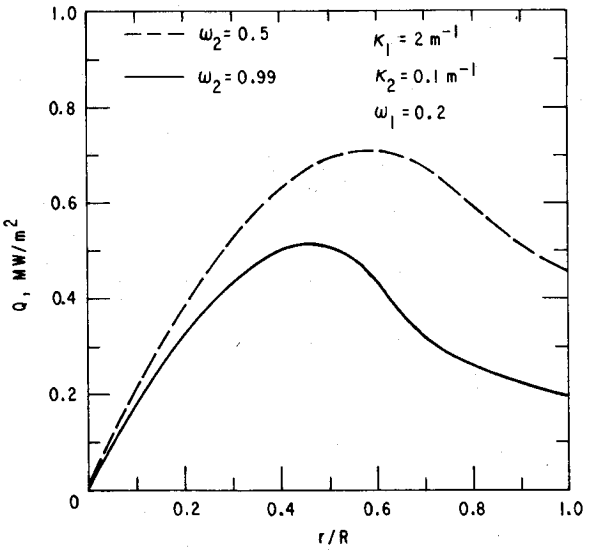

Fig. 3 Effect of ω_2 on heat flux ($\kappa_1 \gg \kappa_2$).

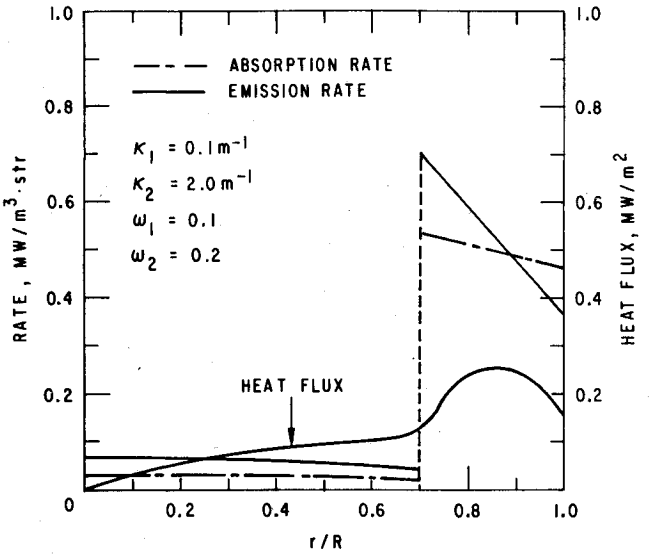

Fig. 4 Spatial variations of absorption and emission rates and heat flux ($\kappa_2 \gg \kappa_1$, $\omega_2 \neq \omega_1$).

general observations made earlier concerning the effect of ω_2 on heat flux and on the extent of the strongly absorbing region apply here as well. The radial variations of the local absorption and emission rates for the situation of $\kappa_2 \gg \kappa_1$ and $\omega_1 \neq \omega_2$, are sketched in Fig. 4. The results of this figure are qualitatively different from the case treated in Fig. 2 where κ_1 was equal to κ_2. The principal difference is that both emission and absorption rates are discontinuous at the interface between regions 1 and 2. The heat flux and the incident radiation are still continuous everywhere in the radiation field, as is the emissive power of the medium. Indeed the continuity of I_b and G implies that the emission rate (κI_b) and the absorption rate ($\kappa G/4\pi$) will be discontinuous wherever κ is discontinuous. This should explain the jump in emission and absorption rates at the interface. In the calculations of Fig. 4, $\kappa_2 \gg \kappa_1$ so that region 2 is a more strongly emitting medium than region 1. This is why the emission and absorption rates are higher in region 2 than in region 1.

Spectral Calculations

In this section results from spectral calculations are presented with carbon dioxide, water vapor, and particles considered to be the major constituents participating in thermal radiation. The intent is to simulate the heat transfer environment of a coal-fired swirl combustor. Since a highly turbulent field is expected to be created by the swirl motion, it is assumed that the concentrations of gaseous species, carbon dioxide and water vapor, are nearly uniform in the radial direction. However, as discussed earlier, the coal particles are expected to exhibit an imhomogeneous distribution because of the centrifugal forces exerted on the particles. Depending upon the degree of swirl and the distance from the point of fuel injection, the extent of segregation of coal particles will be different at different locations in the flowfield.

It is assumed in this section that the radial distribution of the coal particles is already known from the trajectory calculations, and that it can be represented in the form of a step function as

$$n(r_p,r) = n_1(r_p) + [n_2(r_p) - n_1(r_p)]\Theta_+(r - r_0) \qquad (38)$$

In the foregoing equation, n_1 and n_2 are the size distribution functions (number/volume in size range r_p to $r_p + dr_p$) in regions 1 and 2. They are presumed to be given in terms of the generalized fifth-order Rosin-Rammler distribution function.

$$\frac{n_1(r_p)}{N_{01}} = \frac{n_2(r_p)}{N_{02}} = \frac{130}{\langle r_p \rangle}\left(\frac{r_p}{\langle r_p \rangle}\right)^4 \exp\left(-5\frac{r_p}{\langle r_p \rangle}\right) \qquad (39)$$

In order to reduce the number of free parameters, the average particle size in regions 1 and 2 has been fixed at 10 μm. The effect of particle segregation on heat transfer is evaluated by parametrically varying N_{01} and N_{02}. The total number of coal particles and hence the total particle number density, however, is kept fixed in all the computations. A reasonable estimate of the total number density can be made in the following manner. In a coal combustor the air to fuel ratio (by mass) is of the order of 0.13. Then, assuming that the coal particles are in velocity equilibrium with the gas, one has

$$\int_0^R 2\pi r dr \int_0^\infty 4/3\pi r_p^3 \rho_p n u dr_p \Big/ \int_0^R 2\pi r \rho_g u dr = 0.13 \qquad (40)$$

Approximating $\rho_g = 0.95$ kg/m^3 ($p = 5$ atm), $u = $ const, $\rho_p = 1500$ kg/m^3, and using Eq. (38) for radial distribution and Eq. (39) for size distribution of coal particles, Eq. (40)

reduces to the following:

$$N_{02} + (N_{01} - N_{02})(r_0/R)^2 = 1.14 \times 10^4 \ \#/\text{cm}^3 \qquad (41)$$

For consistency in comparison, whenever N_{01} was changed in the calculations to be presented, N_{02} was adjusted simultaneously to ensure that Eq. (41) was always satisfied. Four types of cases were studied: 1) particles are uniformly distributed in regions 1 and 2, i.e., $N_{01} = N_{02}$; 2) all particles are in region 1, i.e., $N_{02} = 0$; 3) equal number of particles are present in regions 1 and 2, i.e., $N_{01}/N_{02} = R^2/r_0^2 - 1$; and 4) all particles are in region 2, i.e., $N_{01} = 0$. Before discussing the results from the four cases, additional information pertaining to the calculation of spectral properties will be discussed. The absorption coefficients of water vapor and carbon dioxide are determined from the exponential wide-band model of Tien.[3] In this model, the absorption coefficient of triatomic gases is characterized by three parameters, C_1, C_2, and C_3, which determine 1) S/d, the mean line width to line spacing ratio at 1 atm; and 2) β, the pressure broadening parameter. The spectral absorption coefficient is then given in terms of S/d and β. There are five vibration-rotation bands in carbon dioxide centered at 15, 10.4, 9.4, 4.3, and 2.7 μm which contribute to radiative heat transfer. Water vapor has four bands centered at 6.3, 2.7, 1.87, and 1.38 μm. For each of these bands in CO_2 and H_2O, the parameters C_1, C_2, and C_3 are given in Ref. 4.

For particles, the efficiency factors for absorption and scattering are computed from Mie theory. The efficiency factor is a function of two nondimensional parameters, $2\pi r_p/\lambda$ and m, the complex refractive index. For coal particles, the data of Foster and Howarth[5] are used to determine the complex refractive index. According to this data, $m = 0.35 - i(1.6)$ for $\lambda < 6$ μm. For $\lambda > 6$ μm,

$$m = 0.35 + 0.733(\lambda - 6) - i[1.6 + 0.125(\lambda - 1.6)] \qquad (42)$$

Since the efficiency factors are functions of particle size, the absorption and scattering coefficients for a cloud of gas containing distributed-size particles is determined as follows:

$$\kappa_{a,\nu} = \kappa_{\nu,CO_2} + \kappa_{\nu,H_2O} + \int_0^\infty \pi r_p^2 Q_a n \, dr_p \qquad (43)$$

$$\kappa_{s,\nu} = \int_0^\infty \pi r_p^2 Q_s n \, dr_p \qquad (44)$$

where n is given by Eq. (39). For evaluating the integrals of Eqs. (43) and (44) the particle-size distribution function is represented in the form of a nine-band histogram. The spatial variation of n is described by Eq. (38) except that in order to simulate the effect of turbulence the particles less that 1 μm in radius are assumed to be uniformly distributed in regions 1 and 2. Unless mentioned otherwise, r_0 is taken as 0.8-m, wall emissivity as 0.7, and the boundary-layer thickness δ as equal to 0.1 m.

The results of the computations for the four cases mentioned earlier are recorded in Table 1. The results are given for wall heat flux as a function of frequency in the form of a histogram. The infrared radiation from carbon-dioxide and water vapor occurs in the 200-8000-cm^{-1} wave-number range, whereas the particles radiate at all frequencies. For the purpose of discussion, the results from the case $r_0 = 0$ will be regarded as the datum for assessing the effect of segregation of particles on heat transfer. This case represents the situation in which all the coal particles are uniformly distributed in regions 1 and 2. It simulates the heat transfer environment of a plug flow combustor. For this case the total heat transfer to the wall is calculated to be 1.14 MW/m^2. In order to estimate the contribution of particles to heat transfer, a computation was made with $r_0 = 0$ but with no particles present. The calculated heat transfer was 0.19 MW/m^2. It can thus be stated that of the total heat transfer, 83% comes from the particles and 17% from the carbon dioxide and water vapor.

Table 1 Histogram representation of spectral heat flux (MW/m^2) for the four cases considered

Wave number, cm^{-1}	Case I, $r_0 = 0$	Case II, $N_2 = 0$	Case III, $N_1 = N_2$	Case IV, $N_1 = 0$
200-810	2.27×10^3	1.17×10^4	2.58×10^2	1.31×10^2
810-1,010	2.51×10^3	1.12×10^4	2.43×10^2	1.22×10^2
1,010-1,328	4.48×10^3	2.97×10^4	6.53×10^2	3.27×10^2
1,328-1,972	1.74×10^4	1.06×10^5	2.54×10^3	1.27×10^3
1,972-3,030	5.95×10^4	1.92×10^5	8.06×10^3	4.06×10^3
3,030-3,730	7.34×10^4	2.52×10^5	8.23×10^3	4.04×10^3
3,730-4,550	1.02×10^5	2.79×10^5	1.17×10^4	5.67×10^3
4,550-6,300	2.20×10^5	4.09×10^5	2.91×10^4	1.36×10^4
6,300-8,000	2.09×10^5	5.40×10^5	2.50×10^4	1.16×10^4
8,000-9,000	9.47×10^4	1.91×10^5	1.47×10^4	6.26×10^3
9,000-10,000	8.09×10^4	1.59×10^5	1.25×10^4	5.12×10^3
10,000-11,000	6.75×10^4	1.27×10^5	1.11×10^4	4.36×10^3
11,000-12,000	5.45×10^4	9.84×10^4	9.55×10^3	3.58×10^3
12,000-13,000	4.23×10^4	7.45×10^4	7.87×10^3	2.84×10^3
13,000-15,000	5.57×10^4	9.59×10^4	1.10×10^4	3.76×10^3
15,000-16,000	1.55×10^4	4.12×10^4	1.11×10^3	3.96×10^2
16,000-17,000	1.22×10^4	2.08×10^4	2.54×10^3	8.03×10^2
17,000-18,000	8.58×10^3	1.46×10^4	1.77×10^3	5.48×10^2
18,000-19,000	5.94×10^3	1.02×10^4	1.22×10^3	3.68×10^2
19,000-20,000	4.05×10^3	7.00×10^3	8.33×10^2	2.47×10^2
20,000-21,000	2.72×10^3	4.77×10^3	5.74×10^2	1.67×10^2
21,000-22,000	1.80×10^3	3.22×10^2	3.92×10^2	1.12×10^2
22,000-23,000	1.18×10^3	2.15×10^3	2.60×10^2	7.35×10^1

The second case studied is one in which all the particles are present in region 1 and none in region 2. This case may simulate the heat transfer environment in the upstream portion of a swirl combustor in which the coal particles are injected near the centerline. Compared to the first case, a 135% enhancement in heat transfer is observed in Table 1. In order to understand this result, it should be recognized first that by virtue of higher temperatures, region 1 is a more strongly emitting region than is region 2. With particles confined in region 1, according to Eq. (41), as compared to the first case the number density of particles in region 1 increases by a factor of $(R/r_0)^2$. This implies a higher absorption coefficient ($\kappa_{\nu 1}$) for all frequencies which leads to a greater emission rate ($\kappa_{\nu 1} I_{b\nu}$). Now, as noted earlier the region close to the wall is a net absorbing region. With no particles present in region 2, the absorption coefficient in the near-wall region is smaller than in the first case which implies a lower absorption rate ($\kappa_{\nu 2} G/4\pi$). The combined influence of increased emission rate in region 1 and reduced absorption rate in region 2 is a net enhancement in heat transfer rate, from 1.14 MW/m^2 in the first case to 2.68 MW/m^2 here.

In the third case studied, the total number of particles in regions 1 and 2 are made equal, i.e., $N_{01}/N_{02} = R^2/r_0^2 - 1$. This means that the number density of particles in region 2 is 1.8 times higher than in region 1. This case may be reflective of an intermediate-swirl combustor. With equal number of particles in regions 1 and 2, Table 1 shows that the heat transfer drops to 0.62 MW/m^2—a 45% decrease in comparison to the heat transfer in the first case. There are two reasons which contribute to the decrease in heat transfer with particles segregated in the wall zone. First, there is a depletion of particles in the highly emitting core, which means that there is a net diminution in the emission rate because of the lower absorption coefficient ($\kappa_{\nu 1}$). Second, the wall region is more densely packed with particles so that the absorption coefficient ($\kappa_{\nu 2}$) increases. Since the wall region is a strongly absorbing region, the net absorption rate ($\kappa_{\nu 2} G_\nu/4\pi$) increases. Weaker emission in the core and stronger absorption in the wall region lead to 45% reduction in heat transfer.

For certain frequencies of radiation the participating medium may become optically thick. This is likely to happen

for frequencies near the band centers of CO_2 and H_2O radiation, and for frequencies corresponding to $\lambda \sim 2\pi r_p$. The likelihood is greater when the particles are closely packed. A parameter that characterizes the approach of a medium to optically thick-limit behavior is ϵ_ν defined as[6]

$$\epsilon_\nu = 1/\{[3(1-\omega_\nu)]^{1/2}\beta_\nu R\} \tag{45}$$

Physically, the nondimensional parameter ϵ_ν, being the ratio of radiation mean free path to the characteristic dimension of the medium, is the Knudsen number for radiation transport. Put another way, it is inversely proportional to the optical thickness. In the optically thick limit, ϵ_ν approaches zero. There are two distinguishing features of the optically thick-limit behavior. First, away from the wall, the emission and absorption rates tend to be in near local equilibrium. Second, near the wall, there is a singularity created owing to the destruction of isotropy in radiation field by the wall. It can be shown that up to $0(\epsilon)$, the heat flux to the wall in the optically thick limit is[5]

$$Q_{r\nu} = -\frac{4\pi}{3\beta_\nu}\frac{1}{1+\gamma[3(1-\omega_\nu)]^{1/2}}\left(\frac{\partial I_{b\nu}}{\partial r}\right)_w \tag{46}$$

The reduction in heat transfer with segregation of particles in the wall zone, as noted in the third case, can be conveniently explained on the basis of Eq. (46). As the particles pile up in the wall zone, the extinction coefficient β_ν increases in magnitude. And if the particle number density is high enough, the optically thick limit is approached in which case the wall heat flux becomes inversely proportional to β_ν and hence decreases. It is interesting to note from Eq. (46), that for the same extinction coefficient (β_ν), the wall heat flux increases with the scattering albedo (ω_ν).

The final case studied is one in which all the particles are present in region 2. This case may simulate the heat transfer environment of a high-swirl combustor. Table 1 shows a drastic reduction in heat transfer for this case, from 1.14 to 0.07 MW/m^2. This reduction is due to the segregation effect of particles and can be explained by the arguments presented in the discussion for the third case and, therefore, need not be repeated. The important thing to note is the considerable influence of the segregation of particles on heat transfer.

Table 2 summarizes the results of the four cases. Here, the range of spectral variations in the extinction coefficients and Knudsen numbers for regions 1 and 2, and the wall heat flux as a function of blackbody emissive power at the core temperature are tabulated. For the case of uniform distribution of particles, the Knudsen number for radiation transport lies in the kinetic range; i.e., the details of the transport process become important here. The wall heat flux is 33% of the blackbody emissive power at temperature T_c. In the second case, where the particles are confined in region 1, the Knudsen number for region 1 lies in the kinetic range to diffusion limit. For region 2, near the band centers of gaseous radiation, the Knudsen number corresponds to the kinetic range. For all other frequencies of radiation, region 2 acts as being optically thin. Thus the core behaves as a blackbody and the wall boundary zone transmits most of the radiation without any significant attenuation. Compared to the first case, the wall heat flux is seen to more than double. In the third case, the Knudsen number for region 2 corresponds to the kinetic range to diffusion limit. A significant degree of attenuation in radiation emitted by the medium takes place in the wall zone, with the result that the wall heat flux reduces to nearly 50% of the first case. In the fourth case, all the particles reside in region 2 and consequently this region acts as being optically thick. The shielding ability of particles is clearly evident in Table 2 in that the wall heat flux reduces to a mere fraction of that in the first case.

Table 2 Radiation transport processes in regions 1 and 2

Case	$\beta_{\nu 1}$, m^{-1}	$\epsilon_{\nu 1}$	$\beta_{\nu 2}$, m^{-1}	$\epsilon_{\nu 2}$	$\frac{Q_w}{(\sigma T_c^4)}$
$r_0 = 0$	1.2-15	0.05-0.67	1.2-1.5	0.05-0.67	0.33
$N_2 = 0$	4-90	0.04-0.40	10^{-3}-4	0.14-43	0.77
$N_1 = N_2$	1-30	0.02-0.71	150-19	5×10^{-3}-0.06	0.18
$N_1 = 0$	10^{-3}-4	10^{3}-0.05	50-300	3×10^{-3}-0.03	0.02

In comparing the four cases studied, the same temperature profile has been used. In reality this would not be the case because of the dependence of the temperature profile on the radiation field. In particular for the case of significant attenuation of radiation in the wall zone, the boundary layer would experience considerable radiative heating. In addition, the temperature of the wall zone will rise owing to the combustion of particles. Therefore the boundary layer will tend to become thinner, which would lead to enhancement of heat flux. Also, in high-swirl combustors for which the particles were found to shield thermal radiation, the convective heat flux is likely to increase with degree of swirl. Therefore the effect of particle segregation in the wall zone on the total heat transfer, convective plus radiative, is not anticipated to be as drastic as envisioned in the calculations presented in this study.

Finally, further work has been done on determining heat transfer in segregated media for the case where the temperature profile is not specified but must be calculated.[7] In that work, the temperature profile is calculated by solving the flow and energy equations in conjunction with the radiation transport equation. An interesting result of that study is the emergence of nonconventional temperature profiles because of the particle segregation effect. For example, for the case of particles segregated in the core region, the study shows the core to experience rapid cooling with the consequent shift of the maximum temperature region away from the core.

Conclusions

A model has been formulated to study the structure of radiation field in a cylindrical medium consisting of two regions of different but uniform absorption and scattering coefficients. The fundamental aspects of the problem are elucidated by considering the case of a gray medium. As an example of the important results, it is shown that for unequal absorption and scattering coefficients in the two regions, both emission and absorption rates are discontinuous at the interface of the two regions, but the heat flux and incident radiation are continuous.

As an applicaton of the model, spectral calculations are performed for a medium with carbon dioxide, water vapor, and coal particles considered as the major species participating in radiation. In order to investigate the effect of particle segregation on heat transfer, the following cases are parametrically studied: uniform distribution of particles in regions 1 and 2; all particles in region 1; equal number of particles in regions 1 and 2; and all particles in region 2. These cases can be related to the heat transfer environment of coal-burning swirl combustors. It is shown through these cases, that the distribution of particles can have an overriding influence on heat transfer. For example, when all the particles were present in the wall region, they were seen to shield the thermal radiation emitted by the medium so much so that the wall heat flux was reduced to a fraction of that for the case of uniform distribution of particles.

Acknowledgment

This work is supported by the U. S. Department of Energy, Magnetohydrodynamic Division.

References

[1] Davison, B. and Sykes, J. B., *Neutron Transport Theory,* Oxford University Press, New York, 1957, pp. 157-173.

[2] Bayezitoglu, Y. and Higenyi, J., "Higher-Order Differential Equations of Radiative Transfer: P_3 Approximation," *AIAA Journal,* Vol. 17, April 1979, pp. 424-431.

[3] Im, K. H. and Ahluwalia, R. K., "Convective and Radiative Heat Transfer in MHD Radiant Boilers," *Journal of Energy,* Vol. 5, Sept.-Oct. 1981, pp. 308-314.

[4] Tien, C. L., "Thermal Radiation Properties of Gases," *Advances in Heat Transfer,* Vol. 5, 1968, pp. 253-324.

[5] Foster, P. J. and Howarth, C. R., "Optical Constants of Carbon and Coal in the Infrared," *Carbon,* Vol. 6, 1968, pp. 719-729.

[6] Ahluwalia, R. K. and Im, K. H., "Structure of Thermal Radiation Field in Optically Thick Limit," to be published in *AIAA Journal.*

[7] Ahluwalia, R. K. and Im, K. H., "Radiative Heat Transfer in Segregated Media," Paper 82-HT-16 presented at the AIAA/ASME Fluids, Plasma, Thermodynamics and Heat Transfer Conference, St. Louis, Mo., June 1982.